A&A 398, 763–773 (2003)
DOI: 10.1051/0004-6361:20021703

Astronomy & Astrophysics

Depolarizing lines in the Sun's spectrum

D. M. Fluri and J. O. Stenflo

Institute of Astronomy, ETH Zentrum, 8092 Zurich, Switzerland

Received 3 April 2002 / Accepted 12 November 2002

Abstract. The majority of all lines in the solar spectrum depolarize the continuum. Here we present a theoretical analysis of the depolarizing lines. In a parameter survey where we vary the details of line formation such as height of formation, we find that absorption and scattering lines have entirely different behavior. While the depolarization by absorption lines rapidly decreases with increasing height of formation, the depolarization by scattering lines increases with height of formation. We interpret the results in terms of a simple qualitative model that contains the relevant physics and support it with quantitative calculations. The main relevant quantities are the anisotropy of the radiation field, which varies over the line profile, and the probability that a photon undergoes polarized scattering above the height where the atmosphere becomes optically thin. For lines with intrinsic polarization we find that the coupling between continuum and line polarization can be neglected.

Key words. line: formation – polarization – radiative transfer – scattering – Sun: atmosphere

1. Introduction

The observations by Stenflo & Keller (1996, 1997) and the atlas recorded by Gandorfer 2000) have revealed the rich structure of the linearly polarized spectrum of the Sun, which is formed by coherent scattering and is known as the "second solar spectrum" (Ivanov 1991). In recent years there have been considerable advances both in observational techniques and in the development of numerical tools to model scattering polarization (Stenflo & Nagendra 1996; Nagendra & Stenflo 1999). It has now become urgent to implement such diagnostic tools so that we can retrieve the information contents of the "second solar spectrum".

The Sun's radiation field is in general polarized at all wavelengths in the visible. In the continuum the polarization is mainly due to Thomson and Rayleigh scattering at free electrons and at neutral hydrogen, respectively. A large fraction of the lines in the solar spectrum depolarize the continuum. In addition, lines with an intrinsic polarizability enhance the degree of polarization when they are formed by coherent scattering. The resulting total polarization has contributions from the continuum, line depolarization, and intrinsic line polarization. The line polarization varies spatially and temporarily due to the influence of the structured magnetic fields via the Hanle effect. To understand the relevant physical processes behind the "second solar spectrum" one needs to have a good knowledge of each contributing process.

In the first survey of the "second solar spectrum" (Stenflo et al. 1983a,b) it was noted that most lines depolarize the continuum polarization and appear as "absorption lines" in terms of linear polarization (Stokes Q/I). To extract the intrinsic line polarization and separate it from the continuum contribution, a simple scaling relation between the absorption profile shapes in Stokes I and in Q/I was adopted, as suggested by the scatter plots of Q/I vs. I in the UV part of the spectrum, where the continuum polarization is large (Stenflo et al. 1983a). This scaling relation is statistical in nature, since it does not account for the individuality of the spectral lines, and no theoretical basis for it has been available.

After the continuum polarization had been theoretically studied and modeled by Fluri & Stenflo (1999a), they could begin exploring the depolarizing lines, in particular the relation between the line profile shape in terms of intensity and degree polarization (Fluri & Stenflo 1999b). Additional insight into the behavior of depolarizing lines has been obtained by Fluri & Stenflo (2001) although only for absorption lines. In the present paper we extend our study of depolarizing lines from absorption to scattering lines. The objective is to gain insight into how depolarization originates.

Apart from deepening our understanding of the "second solar spectrum" a study of depolarizing lines is needed for further reasons. The zero point of the polarization scale is not determined by the observations to sufficient accuracy. If we could find a simple correlation between the profile shapes in intensity and degree of polarization for depolarizing lines, then we could infer the correct zero point from the Stokes spectra (Stenflo et al. 1998). The purpose of the present paper may therefore be summarized by the following two questions: how are depolarizing lines formed, and is there a simple relation between the intensity and polarization profiles that is always valid?

In Sect. 2 we introduce the transfer equation and the formalism used. Section 3 is devoted to lines without intrinsic

Send offprint requests to: D. M. Fluri,
e-mail: dfluri@astro.phys.ethz.ch

polarization to allow the depolarization effects to be isolated. The aim is to survey the behavior of depolarizing lines when the details of the line formation process are varied. Lines with intrinsic polarization are treated in Sect. 4 to study the non-linear effects when both line and continuum polarization interact with depolarization. The conclusions are presented in Sect. 5.

2. Modelling depolarization

2.1. Transfer equation

We consider a plane-parallel, static solar atmosphere with homogeneous layers. It is sufficient to describe the radiation field by the Stokes vector $\boldsymbol{I}=(I, Q)$ since we neglect magnetic fields and since we define the coordinate system such that Stokes Q represents linear polarization parallel to the nearest solar limb. The continuum optical depth is defined as

$$\mathrm{d}\tau_\mathrm{c} = -(\kappa_\mathrm{c}+\sigma_\mathrm{c})\,\mathrm{d}z, \tag{1}$$

where κ_c is the continuum absorption coefficient, σ_c the continuum scattering coefficient, and z the geometric height. To model depolarizing lines we solve the polarized radiative transfer equation

$$\mu\frac{\partial \boldsymbol{I}_x}{\partial\tau_\mathrm{c}} = \left(\frac{\phi_x}{\beta}+1\right)(\boldsymbol{I}_x-\boldsymbol{S}_x). \tag{2}$$

Here and in the following the depth and angle dependence of variables are in general omitted, while the frequency dependence is expressed by subscript x. The frequency x is always given in units of the Doppler width ($x=0$ at line center). As usual, $\mu=\cos\vartheta$, where ϑ is the angle between the direction normal to the surface and the line of sight. The variable ϕ_x is the Voigt function with its area normalized to unity. The ratio of continuum to line opacity β is given by

$$\beta = \frac{\kappa_\mathrm{c}+\sigma_\mathrm{c}}{\kappa_\ell}, \tag{3}$$

where κ_ℓ is the integrated line absorption coefficient. If we introduce the ratio

$$\rho = \frac{\sigma_\mathrm{c}}{\kappa_\mathrm{c}+\sigma_\mathrm{c}}, \tag{4}$$

we can write the total source vector $\boldsymbol{S}_x$ as

$$\boldsymbol{S}_x = \frac{(\phi_x/\beta)\boldsymbol{S}_{\ell,x}+(1-\rho)\,\boldsymbol{B}_\mathrm{th}+\rho\boldsymbol{S}_\mathrm{c}}{(\phi_x/\beta)+1}. \tag{5}$$

The vector $\boldsymbol{B}_\mathrm{th}=(B_{x_0},0)$ is the thermal source term of the continuum with the Planck function B_{x_0} at line center. Rayleigh and Thomson scattering in the continuum enter via

$$\boldsymbol{S}_\mathrm{c} = \frac{1}{2}\int_{-1}^{+1}\hat{\boldsymbol{P}}(\mu,\mu',W_\mathrm{eff}=1)\boldsymbol{I}_x(\mu')\,\mathrm{d}\mu', \tag{6}$$

where we have used the property that the radiation field does not depend on azimuth when the magnetic field is zero. The scattering processes described by Eq. (6) are frequency coherent. The phase matrix is given by

$$\hat{\boldsymbol{P}}(\mu,\mu',W_\mathrm{eff}) = \hat{\boldsymbol{P}}^{(0)}+\frac{3}{4}W_\mathrm{eff}\,\hat{\boldsymbol{P}}^{(2)}(\mu,\mu'), \tag{7}$$

where W_eff is the effective polarizability parameter. The matrix $\hat{\boldsymbol{P}}^{(0)}$ represents unpolarized, isotropic scattering (first element one, all other elements zero), while $\hat{\boldsymbol{P}}^{(2)}$ accounts for the scattering of the linear polarization and is given explicitly e.g. in Stenflo (1994), where the notation $\boldsymbol{P}^2$ is used. The line source function is given by

$$\boldsymbol{S}_{\ell,x} = \frac{1-\epsilon}{2\phi_x}\int_{-\infty}^{+\infty}\int_{-1}^{+1}\hat{\boldsymbol{R}}(x,x';\mu,\mu')\boldsymbol{I}_{x'}(\mu')\,\mathrm{d}\mu'\mathrm{d}x'+\epsilon\boldsymbol{B}_\mathrm{th}. \tag{8}$$

The parameter ϵ determines how much of the line is formed by absorption and how much is formed by scattering. Pure absorption lines have $\epsilon=1.0$, pure scattering lines $\epsilon=0$.

In our radiative transfer code we have implemented the redistribution matrix given by Bommier (1997) in her approximation level III for weak magnetic fields. Since we assume a non-magnetic atmosphere it simplifies to

$$\begin{aligned}\hat{\boldsymbol{R}}(x,x';\mu,\mu') &= k_\mathrm{c}R_\mathrm{II}(x,x')\hat{\boldsymbol{P}}(\mu,\mu',W_\mathrm{eff}=W_2)\\ &+\ (1-k_\mathrm{c})R_\mathrm{III}(x,x')\hat{\boldsymbol{P}}\left(\mu,\mu',W_\mathrm{eff}=\frac{k_\mathrm{c}^{(2)}-k_\mathrm{c}}{1-k_\mathrm{c}}\,W_2\right).\end{aligned} \tag{9}$$

The scalar functions R_II and R_III represent angle averaged frequency redistribution in the standard notation of Hummer (1962). The polarization parameter W_2 depends only on the total angular momentum quantum numbers J and J' of the lower and upper level. A tabulation of W_2 can be found for various electric-dipole transitions in Landi Degl'Innocenti (1984). The collisional parameters are defined as in Stenflo (1994), except that here we also take inelastic collisions into account

$$k_\mathrm{c} = \frac{\Gamma_\mathrm{R}+\Gamma_\mathrm{I}}{\Gamma_\mathrm{R}+\Gamma_\mathrm{I}+\Gamma_\mathrm{E}}, \tag{10}$$

$$k_\mathrm{c}^{(2)} = \frac{\Gamma_\mathrm{R}+\Gamma_\mathrm{I}}{\Gamma_\mathrm{R}+\Gamma_\mathrm{I}+D^{(2)}}. \tag{11}$$

Here Γ_R represents the radiative de-excitation rate, Γ_E the elastic collision rate, Γ_I the inelastic collision rate, and $D^{(2)}=0.5\Gamma_\mathrm{E}$ the rate of depolarizing elastic collisions.

2.2. Line opacity

The definition of the line opacity has to be done with special care. Our aim is to study the behavior of different depolarizing lines in a realistic solar environment. For this we need to introduce the line opacity both in an artificial way for a parameter survey of idealized lines as well as for real lines.

We use the semi-empirical average quiet Sun model C of Fontenla et al. (1993). Continuum opacities κ_c and σ_c are obtained for 5000 Å with the opacity package currently built into the MULTI code (Carlsson 1986), which is based on the Uppsala opacity package of Gustafsson (1973).

In Sect. 3 we consider idealized lines in order to have clearly defined circumstances, which allow unambiguous interpretations. For one type of lines, labeled "ME" for Milne-Eddington, the line opacity κ_ℓ is fixed by the value of β, which is kept constant throughout the atmosphere. For a second type of lines the depth dependence of κ_ℓ is given by a Gaussian

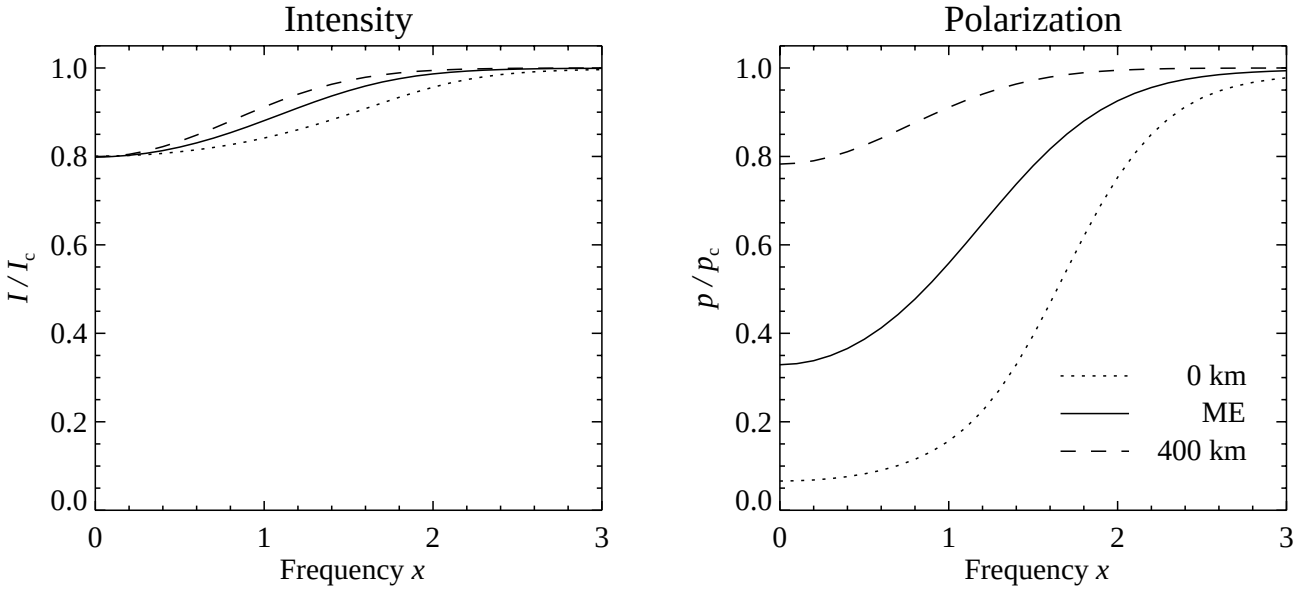

Fig. 1. Depolarization of absorption lines. The intensity (left panel) and linear polarization (right panel) of pure absorption lines ($\epsilon = 1.0$) are plotted for $\mu = 0.1$. The continuum opacity at 5000 Å has been used. The lines differ only in the definition of the line opacity. The "0 km" and the "400 km" lines have the line opacity centered around a height of 0 km and 400 km, respectively, while the ratio of line to continuum opacity for the "ME" line remains constant throughout the whole atmosphere. The absolute value of the line opacity is chosen to give the same relative line depth of 0.2 in intensity in all the three cases. Still the resulting depolarization differs greatly.

distribution in geometric height with a $FWHM$ of 200 km. The geometric height at the maximum of κ_ℓ is used to label the corresponding line, e.g. "0 km", or "400 km".

In Sect. 4 we use the line opacity of a real line, namely the Fe I line at 5956.7 Å (transition $a^5\mathrm{F}_5 - z^7\mathrm{P}^\mathrm{o}_4$). Nonetheless, the other parameters except the atomic mass remain unchanged, like the model atmosphere, or, in particular, the wavelength of 5000 Å at which the continuum opacity is defined. Thus we do not claim to reproduce the observed Fe I line, since the only objective is to replace the somewhat artificial definition of κ_ℓ in Sect. 3 with a realistic distribution, without changing the other parameters.

2.3. Numerical method

The transfer Eq. (2) is solved using the PALI code that has been developed and extended in a series of papers (Faurobert-Scholl et al. 1997; Paletou & Faurobert-Scholl 1997; Nagendra et al. 1998, 1999, 2000; Fluri & Nagendra 2003). It is basically an Approximate Lambda Iteration method using a local approximate operator (Olson et al. 1986) but for a polarized radiation field.

The code used in the present paper is an extension of the version introduced in Fluri & Nagendra (2003). Here we have in addition implemented polarized scattering in the continuum, which adds extra terms to most equations of that paper. We however refrain from writing down all these equations again.

As for computational details, we have used a logarithmic optical depth grid with 10 points per decade, 5 Gaussian latitude angles, and a 101 point non-uniform frequency grid with the last frequency point at $x = 1000$. Frequency is given with respect to line center in units of the Doppler width at the temperature minimum.

3. Lines without intrinsic polarization

Many lines in the solar spectrum just depolarize the linear polarization in the continuum without showing any sign of intrinsic polarization. The present section addresses the behavior of such lines. The aim is to understand the observed depolarization for a whole range of different lines, such as absorption and scattering lines characterized by various parameters that are introduced through different definitions of the line opacity. First we will survey the resulting depolarization when moving around in parameter space, and then provide interpretations of the results.

In the present section the line opacity of all the lines plotted has been scaled such that the resulting relative line depth of Stokes I at line center is exactly 0.2. By fixing this parameter it becomes easier to compare different lines and to identify the relevant processes that lead to depolarization, without confusing these processes with line-strength effects.

Apart from the line opacity and ϵ, all parameters have been kept fixed. The radiative transition rate Γ_R has the value of the classical harmonic oscillator, i.e., $8.9 \times 10^7\ \mathrm{s}^{-1}$ at 5000 Å. The rate of elastic collisions is determined according to the Lindholm theory for Van der Waals interactions between the considered atom and neutral hydrogen or neutral helium (see e.g. Mihalas 1978). We have assumed an atomic weight of 40, which would correspond to Calcium. The microturbulent velocity, which enters in the Doppler width, has been set to the constant value of $0.7\ \mathrm{km\,s}^{-1}$.

3.1. Parameter survey

Figure 1 shows the line profiles of absorption lines with $\epsilon = 1$ in the direction $\mu = 0.1$. The line opacity in the "0 km" line has

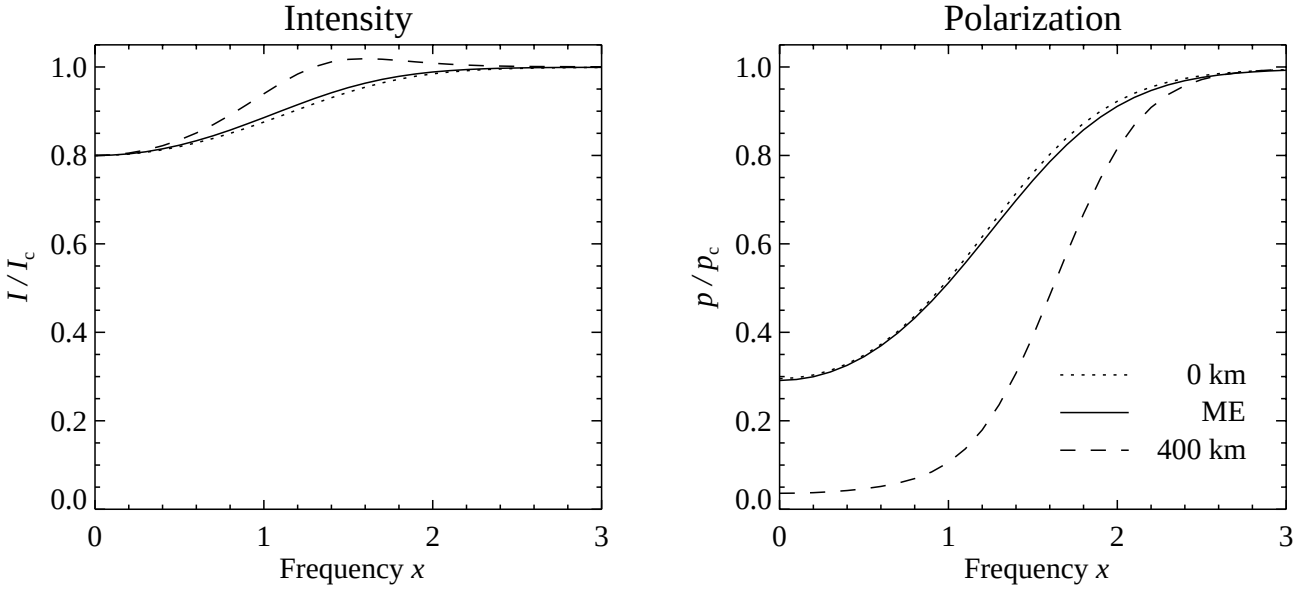

Fig. 2. Depolarization of scattering lines. The same parameters as in Fig. 1 have been used to compute these lines, except that we choose $\epsilon = 0$ to obtain pure scattering lines. The intrinsic line polarizability is set to zero ($W_2 = 0$). All three lines have the same relative line depth of 0.2 in intensity at line center. The depolarization for the "400 km" line is much stronger than for the "0 km" line, in contrast to the absorption lines of Fig. 1.

the maximum value $\kappa_{\ell,\max} = 1.38 \times 10^{-6}$ cm^{-1}, which is reached at the geometric height of 0 km as indicated by its label. The "400 km" line is obtained with $\kappa_{\ell,\max} = 4.67 \times 10^{-9}$ cm^{-1} at 400 km. The "ME" line is characterized by the constant value $\beta = (\kappa_c + \sigma_c)/\kappa_\ell = 2.67$. The emergent polarization $p = Q/I$ relative to its continuum value $p_c = Q_c/I_c$ varies significantly between the three lines although they have the same relative line depth in intensity. The "400 km" line depolarizes the continuum only slightly, while the "0 km" line produces almost complete depolarization. We therefore immediately see that it is not possible to find a simple relation between line depth in Stokes I and degree of depolarization. As the only difference between the three lines is the depth dependence of κ_ℓ, the details of line formation has a decisive influence on the emerging polarization.

In Fig. 2 the profiles of pure scattering lines with $\epsilon = 0$ are given, again for the line-of-sight defined by $\mu = 0.1$. Note that the intrinsic line polarizability W_2 has been set to zero. Basically the same lines as in Fig. 1 are illustrated, with the only difference that the line opacities had to be renormalized in order to again obtain the relative line depth of 0.2. For these scattering lines the values of $\kappa_{\ell,\max}$ are 3.93×10^{-7} cm^{-1} for the "0 km" line and 7.08×10^{-8} cm^{-1} for the "400 km" line, while the constant ratio of continuum to line opacity in the "ME" line is $\beta = 2.94$. The resulting depolarization is practically identical in the "0 km" and the "ME" lines. Almost complete depolarization is achieved in the "400 km" line. Interestingly the scattering and absorption lines behave in opposite ways. For scattering lines it is the "400 km' line that has a nearly unpolarized radiation field at line center, while it is the "0 km" line that is nearly unpolarized if the line is formed by absorption.

The dependence on height of formation is brought out more explicitly in Fig. 3. We have solved the radiative transfer equation for many different lines formed at different heights. The line opacity has been defined as for the "0 km" and the "400 km" lines of Figs. 1 and 2. The maximum of κ_ℓ occurs at a certain height and falls off to both sides according to a Gaussian distribution with a $FWHM$ of 200 km. Again, the absolute value of κ_ℓ has been scaled to yield a relative line depth of 0.2 in the intensity profile.

The left panel of Fig. 3 shows the ratio of polarization p to intensity I for $x = 0$, where both p and I are given in units of their continuum values. Because $I/I_c = 0.8$ and because the degree of continuum polarization is also the same for all the computed lines, the quantity plotted in the left panel is really a measure of the polarization at line center. A value of unity corresponds to no depolarization at all, while a value of zero represents complete depolarization. The data are plotted as functions of the geometric height at which the line contribution function of the intensity $C_{I,\text{line}}$ has its maximum. This height serves as a measure for the height of formation of the line. The function $C_{I,\text{line}}$ is determined in the direction of $\mu = 0.1$.

Interestingly the height dependence of absorption and scattering lines differ dramatically. Depolarization in scattering lines increases steadily with height from moderate values to almost complete depolarization in the upper photosphere. Absorption lines on the other hand depolarize the continuum strongly if they are formed deep in the atmosphere, while they become almost invisible in linear polarization if they originate from higher layers. The transition from large to small depolarization is much more rapid than for scattering lines and occurs over as little as 50 km.

While the formation height is the relevant physical quantity, it has not been the input parameter. Rather it is the height of the maximum of the line opacity κ_ℓ that we define at the beginning. The translation between the two quantities is shown in the right panel of Fig. 3. Note in particular that even the "0 km" line is formed above 200 km. This is due to the circumstance that the

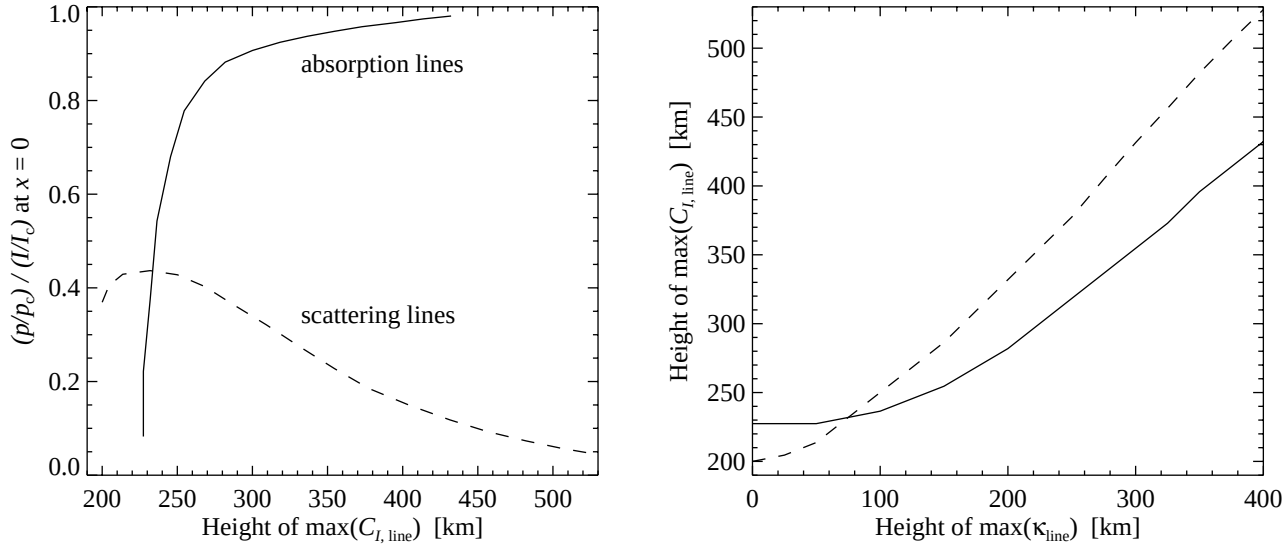

Fig. 3. Height dependence of depolarization in absorption (solid) and scattering (dashed) lines. The line opacity κ_ℓ is defined artificially by a Gaussian distribution around a certain atmospheric height, which is varied from 0 km to 400 km. The absolute value of κ_ℓ is defined such that $I/I_c = 0.8$ at line center. For each κ_ℓ the height of the maximum of the Stokes I line contribution function $C_{I,\mathrm{line}}$ (right panel) is computed by solving the radiative transfer problem. The resulting depolarization is plotted in the left panel. Polarization and $C_{I,\mathrm{line}}$ are determined at line center for $\mu = 0.1$. Note that p_c and I/I_c have the same values for all the lines. While depolarization in scattering lines increases with height, absorption lines have the opposite behavior.

line-of-sight optical depth in the continuum reaches a value of unity at 160 km for $\mu = 0.1$. Below, the continuum is optically thick. Since for line frequencies there is additional opacity, the formation height is shifted still higher for line photons.

3.2. Interpretation

It is now possible to interpret the results obtained in the parameter survey of Sect. 3.1 to get a qualitative and conceptual understanding of depolarization. In the following we will discuss a simple model that contains all the relevant physics involved in the process of depolarization. We consider absorption and scattering lines separately before validating the qualitative explanation with calculations that take the anisotropy of the radiation field into account.

Absorption lines

Figure 4 illustrates schematically regions in the atmosphere where different types of opacity are of importance at different frequencies. We distinguish between continuum absorption opacity, line opacity, and opacity due to polarized continuum scattering. The vertical scale gives the continuum optical depth τ_c. The left panel represents a line formed deep in the atmosphere, while the right panel corresponds to a line that originates in high layers of the atmosphere.

Below $\tau_c = 1$ the continuum is optically thick. If scattering occurs in these layers (which is certainly the case), the resulting polarization will be destroyed again by absorption processes in the layers above. Polarization can start to be built up only at heights where the atmosphere is becoming optically thin in the continuum. These are the layers that are marked as polarized scattering in Fig. 4. We have however not extended this scattering region to the top, because the scattering coefficient σ_c that is the source of the emergent polarization decreases exponentially due to the drop in density.

In reality it is not possible to clearly separate the layers where the continuum is optically thick and where polarized scattering occurs. The contribution functions of Stokes I and Q do indeed overlap in the continuum (Fluri & Stenflo 1999a). The maximum of C_Q however lies higher than the maximum of C_I. Qualitatively it is therefore justified to separate the two regions, although only radiative transfer computations can give us the complete and correct picture.

Let us first consider the case described by the left panel of Fig. 4 and assume that the line opacity is entirely due to absorption ($\epsilon = 1$). In the continuum, which is nearly reached at $x = 3$, linear polarization is built up between $\tau_c = 1$ and the top of the scattering layer. The closer we move to the line center, the larger becomes the line absorption. Photons can only escape from higher layers, and the remaining portion inside the slab that is available to the build-up of polarization diminishes. The probability that a photon is scattered before emerging from the top of the atmosphere is thus reduced, which in turns leads to a reduced degree of polarization in the line.

If the line is formed above the layer of polarized scattering (right panel of Fig. 4) the situation changes. For all frequencies the same degree of polarization emerges from the scattering layer, before the photons enter the slab that contains the line opacity. If the line is optically thin it reduces Stokes I and Q by the same factor by absorption. Therefore the ratio Q/I remains constant. If in addition the temperature in these layers is much smaller than in the lower photosphere, the additional reemitted radiation due to thermal emission can be neglected. Thus the resulting polarization emerging at the top of the atmosphere is the same for all frequencies.

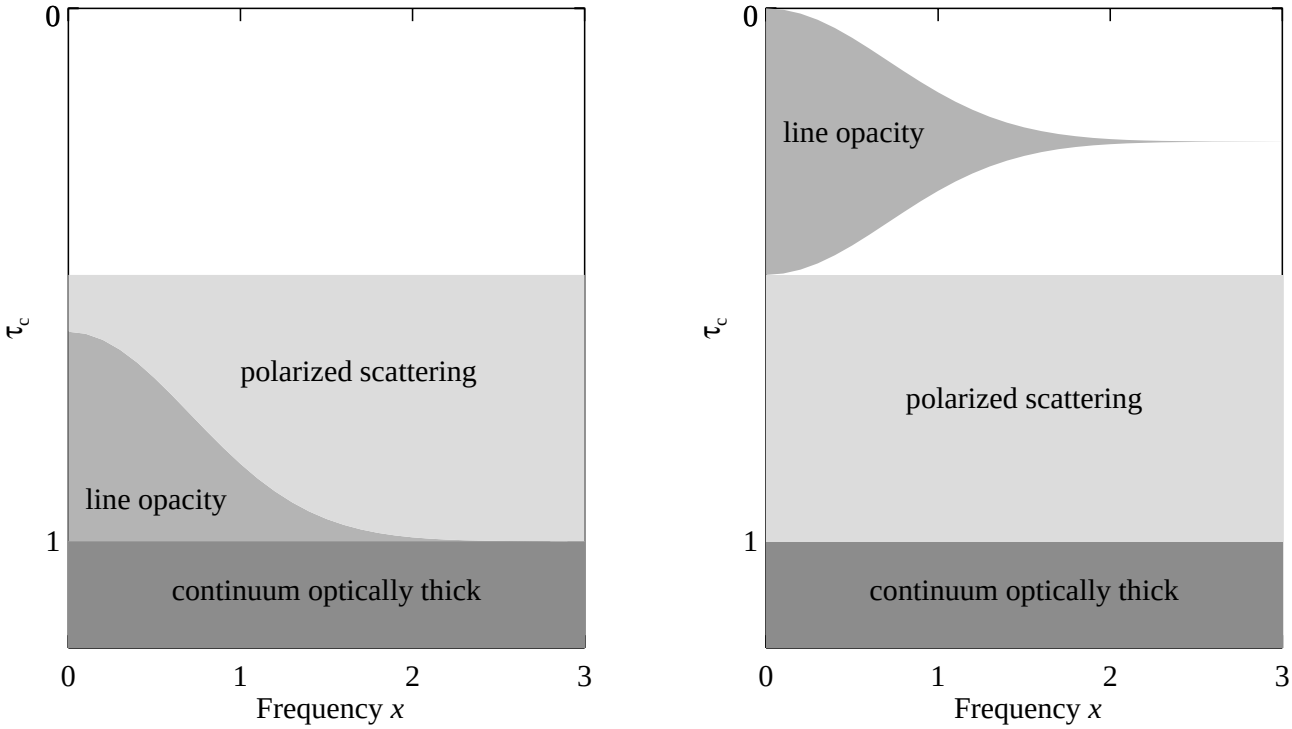

Fig. 4. Schematic illustration of regions in the atmosphere with three different sources of opacity, given as functions of frequency, used to qualitatively explain the height dependence of the depolarization (see text). Two extreme cases with line opacity deep (left panel) and high (right panel) in the atmosphere are represented. We assume that the line opacity can either cause absorption or unpolarized scattering. Below $\tau_c = 1$ the atmosphere is optically thick in the continuum. Any polarization formed below would be destroyed again by absorption in these layers. Above, where the atmosphere becomes transparent, the radiation field gets polarized by Thomson and Rayleigh scattering.

The qualitative picture given above neglects the frequency dependence of the anisotropy of the radiation field. After a discussion of scattering lines we will return to the anisotropy effects.

Scattering lines

Let us now assume that the line opacity in Fig. 4 refers to unpolarized scattering, i.e., $\epsilon = 0$ and $W_2 = 0$. If the line is formed deep in the photosphere the same arguments as for absorption lines apply. The atmosphere becomes optically thin only at the upper end of the line opacity region. Below, any polarization would be destroyed, either by continuum absorption or by unpolarized line scattering. The emerging polarization at the top of the atmosphere scales with the remaining path length inside the polarized scattering layer, which is much reduced when moving towards the line center.

If the line originates from high layers (right panel of Fig. 4) the situation becomes different as compared with absorption lines. Let us first consider the case of an optically thin line. Then Stokes Q is reduced by the fraction of the radiation field that undergoes unpolarized line scattering. Stokes I on the other hand is not altered that much, because the photon number is conserved in scattering. The closer we get to the line center, the smaller is the ratio Q/I, i.e., the continuum becomes depolarized. If the line becomes optically thick all line photons reaching an observer at the top are due to unpolarized line scattering. As the line opacity lies above the polarized scattering layer of the continuum, we then obtain a completely depolarized line at $x = 0$.

An example of an optically thick line formed at large height is the "400 km" line in Fig 2. We recall that the maximum line opacity used for this line has been $\kappa_{\ell,\max} = 7.08 \times 10^{-8}$ cm^{-1}. If we would have chosen a smaller value, e.g. the $\kappa_{\ell,\max}$ used for the "400 km" absorption line of Fig. 1, then the line would be optically thin also for $\mu = 0.1$. Such a scattering line would be invisible in the intensity spectrum but would depolarize the continuum significantly ($p/p_c = 0.6$ at line center), in agreement with the arguments above.

Geometric polarization factor

A necessary condition to get an emerging radiation field that becomes linearly polarized by scattering processes is that the radiation field is anisotropic in the layer where the scattering occurs. One of the arguments given in the last two subsections has been based on the path length inside the polarized scattering layer. The anisotropy of the radiation field has only been included implicitly by assuming that the continuum scattering really polarizes the radiation. In this subsection we will examine the influence of the anisotropy more quantitatively. As we will see, the anisotropy varies across the line. At least for lines formed deep in the atmosphere it is the combination of anisotropy and scattering path length that is responsible for the final degree of polarization.

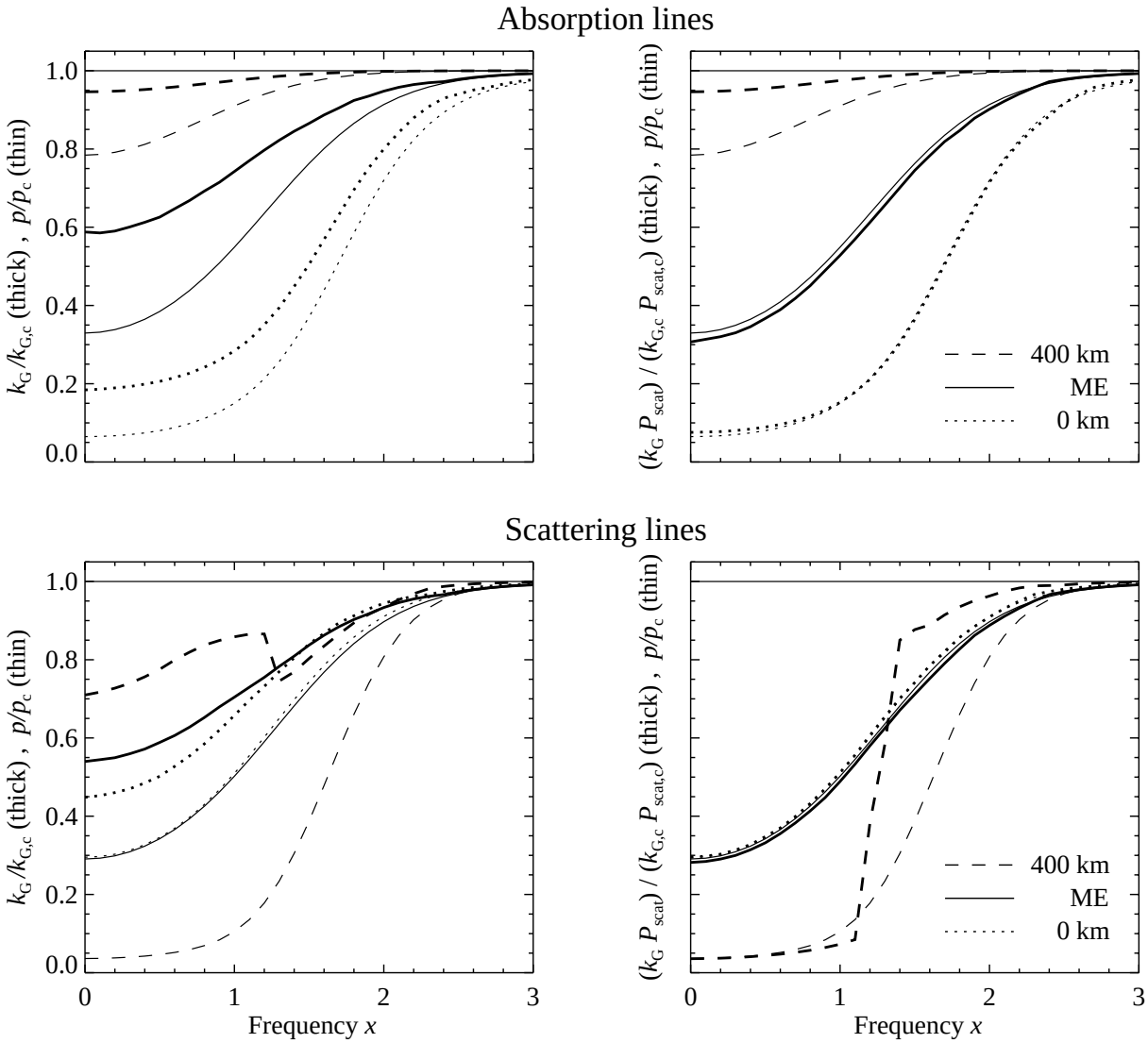

Fig. 5. Influence of the anisotropy of the radiation field and the optical thickness of the scattering layer. In the upper half the results for the absorption lines of Fig. 1 are plotted. The lower half shows the results for the scattering lines of Fig. 2. The thin lines represent the emergent polarization at the top of the atmosphere. In the left panel the geometric polarization factor k_G (thick lines) relative to its continuum value is given. It represents the influence of the anisotropy of the radiation field on the emergent polarization. The factor k_G is given at the height where the Stokes Q contribution function C_Q has its maximum. In the right panel k_G is multiplied with the quantity P_{scat} defined in Eq. (14). The variable P_{scat} accounts only for the scattering opacity in the continuum and gives the probability that the scattering process described by k_G occurs. All curves refer to $\mu = 0.1$. The thin, solid, horizontal line at 1.0 marks the continuum level. Note that all variables with subscript "c" indicate continuum values.

A good measure of the anisotropy of the radiation field and the expected degree of polarization is the geometric polarization factor k_G, which has been introduced by Stenflo (1982) as

$$k_G = \frac{3}{16} \frac{\left(1-\mu^2\right)}{I(\mu)} \int_{-1}^{+1} \left(1 - 3\mu'^2\right) I(\mu')\, \mathrm{d}\mu'. \qquad (12)$$

Basically it is the average Stokes Q component that is produced by a single dipole scattering event with an unpolarized incident radiation field. Mathematically it is obtained when multiplying the Rayleigh phase matrix with the incident Stokes vector and integrating over all incident angles. Because the last scattering process before a photon escapes from the solar atmosphere is by far the most important one, k_G should be an approximate measure of the final degree of polarization.

The frequency dependence of k_G (thick lines) normalized to the continuum value is illustrated to the left in Fig. 5. The upper half of the figure corresponds to the same three absorption lines that were given in Fig. 1, while the lower half of Fig. 5 refers to the three scattering lines of Fig. 2. For comparison the emergent polarization (thin lines) is also plotted.

The polarization factor k_G is determined for the layer, where the Stokes Q contribution function C_Q in the direction $\mu = 0.1$ reaches its maximum. This is a reasonable choice, since the main scattering contributions occur around the height of maximum C_Q. It is the incident radiation field at these levels that should be used in Eq. (12). Note that this geometric

height is in general frequency dependent. The disagreement between k_G and p is however significant (left side of Fig. 5). The geometric polarization factor k_G may explain about half the amount of depolarization.

However, on the basis of the schematic model of Fig. 4 we have argued that for lines formed deep in the atmosphere the path length in the polarized scattering layer is of relevance. This path length corresponds to the probability that a continuum scattering process occurs. It is given by the optical depth scale

$$d\tau_s = -\sigma_c \, dz. \tag{13}$$

The subscript "s" refers to scattering in the continuum. Let us denote by $\tau_s(C_Q)$ the optical depth in this scale at the height of max (C_Q). Then, along the line-of-sight, the intensity is reduced by a factor $e^{-\tau_s(C_Q)/\mu}$ due to continuum scattering, and the quantity

$$P_{scat} = 1 - e^{-\tau_s(C_Q)/\mu}, \tag{14}$$

approximately corresponds to the scattering probability we are looking for.

While the factor k_G represents the polarization after one scattering process, P_{scat} is the probability that such an event really occurs. The product of the two quantities should therefore approximate the observed polarization:

$$p \approx k_G P_{scat} = k_G \left(1 - e^{-\tau_s(C_Q)/\mu}\right). \tag{15}$$

This quantity is plotted in the panels to the right in Fig. 5. As expected it agrees well with the emerging polarization for the "ME" and the "0 km" absorption and scattering lines. All these lines are optically thick below the height of line formation and can therefore be described in terms of the simplified model in the left panel of Fig. 4. In particular the "ME" and the "0 km" scattering lines, which have nearly identical polarization profiles, confirm the validity of our interpretation. The difference in the polarization factor k_G is compensated for by the scattering probability factor P_{scat}.

A special case is the "400 km" scattering line. The jump around $x = 1.3$ in k_G and in the product $k_G P_{scat}$ occurs because the line becomes optically thick at that frequency. The height of max (C_Q) jumps from about 200 km to almost 500 km. The factor k_G, which is evaluated at this height, changes significantly, at the same time as the remaining optical thickness due to continuum scattering $\tau_s(C_Q)$ diminishes abruptly. In the line core the observed polarization is well fitted by the simple model of Eq. (15) because the line is optically thick. For larger frequencies x, where the line is optically thin, the unpolarized line scattering replaces some fraction of the polarized photons by unpolarized radiation. This mechanism that reduces Stokes Q has not been included in Eq. (15). The degree of polarization is therefore overestimated.

Similarly the "400 km" absorption line is not well fitted by the approximation of Eq. (15). While the optically thin line reduces Stokes I and Q by the same factor and leaves p unchanged, the thermal emission at this height cannot be neglected. Although the line is formed around the temperature minimum it adds some thermal contribution to I, which results in a slight overall depolarization.

4. Lines with intrinsic polarization

For lines with an intrinsic polarizability the situation becomes more complex. Not only do we have the polarized continuum that is depolarized, but also line polarization which is added. If a magnetic field is present the line polarization is further modified by the Hanle effect. The polarized transfer Eq. (2) couples the continuum and line polarization in a non-linear way. Because many of the spectral lines observed in the second solar spectrum have intrinsic polarizations that are of the same order of magnitude as the polarization of the continuum (see e.g. Gandorfer 2000), we need to clarify the role of the non-linear effects due to the coupling between line and continuum in order to be able to interpret the observed polarized profiles.

4.1. Atomic data for Fe I

To explore the interaction between line and continuum polarization we choose pure scattering lines ($\epsilon = 0.0$) with an intrinsic polarizability $W_2 \geq 0.0$ while taking the polarized continuum into account. We want to retain as many parameters as possible from the survey of Sect. 3 but refrain from defining the line opacity artificially as in that section. To introduce more realism we will here use the line opacity of a real line. We have chosen the Fe I line at 5956.7 Å that is due to the transition $a^5F_5 - z^7P^o_4$. The line opacity κ_ℓ for this line is calculated with the MULTI code of Carlsson (1986) for an 18 level Fe I model atom with 17 transitions. MULTI solves the rate equations and the radiative transfer equation simultaneously for a multilevel atom while disregarding polarization.

It is not our intention here to model a specific line. We only want to use a realistic depth dependence of the line opacity. Therefore the other parameters that were used in Sect. 3 are retained. The same model atmosphere is used, and the continuum opacity is still computed for 5000 Å. In particular the same value for $\Gamma_R = 8.9 \times 10^7 \, s^{-1}$ is adopted. The correct atomic weight of Fe, 58.85, enters the calculation of the elastic collision rate Γ_E.

4.2. Coupling of line and continuum polarization

The intensity and polarization of the Fe line obtained with the parameters given above are plotted in Fig. 6 for various values of the intrinsic polarizability W_2. We have chosen W_2 such that the degree of polarization in the line is comparable to the continuum polarization.

The line with $W_2 = 0.00$ (solid) is an example of a pure depolarizing line without intrinsic polarization. From our survey in Sect. 3 it is not surprising that this scattering line depolarizes the continuum almost completely. Note that the Fe I line considered here is stronger than the lines surveyed in Sect. 3.

Increasing the value of W_2 we add polarization with respect to the $W_2 = 0.00$ line. The curve for $W_2 = 0.02$ (dash-dotted) shows some depolarization around $x = 1.5$ and a total polarization at line center that is slightly larger than in the continuum. A similar effect but generally more pronounced is observed in many of the much stronger lines in the "second solar

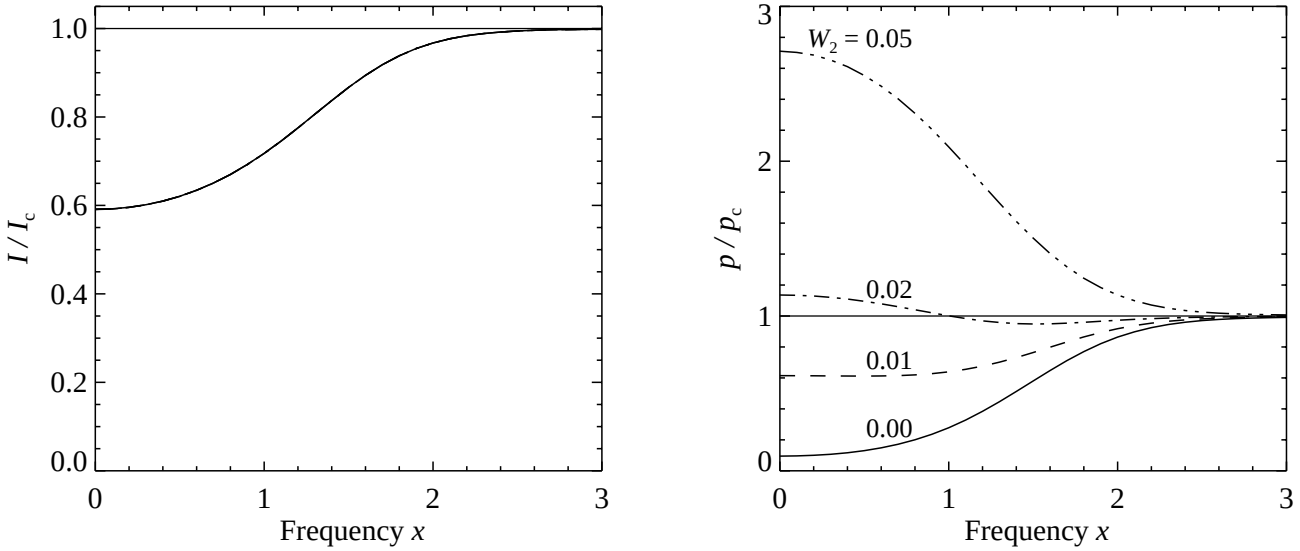

Fig. 6. Intensity and linear polarization in the Fe I line for different values of W_2. The line-of-sight is in the direction of $\mu = 0.1$. All parameters are the same as in Fig. 2 except for the atomic mass and the line opacity, which are defined by the Fe I line. This allows us to study depolarization and line polarization for realistic atomic parameters. We have chosen the values of W_2 such that the contributions to the total polarization from continuum and line polarization as well as from depolarization are of the same order of magnitude. The intensity profiles are identical for the four different lines. In both panels the thin horizontal line indicates the continuum level.

spectrum", with a polarization peak in the line core combined with substantial depolarization in the wings.

In the presence of a weak turbulent magnetic field with an isotropic angular distribution of field vectors $\boldsymbol{B}$ the effective polarizability $W_{\rm eff}$ in the phase matrices of Eq. (9) should be replaced by

$$W_{\rm eff}(\boldsymbol{B}) = W_{\rm eff}(\boldsymbol{B}=0)\left[1 - \frac{2}{5}\left(\sin^2\alpha_1 + \sin^2\alpha_2\right)\right]. \qquad (16)$$

The variables α_1 and α_2 depend on the magnetic field strength and on the transition rates $\Gamma_{\rm R}$ and $\Gamma_{\rm E}$ (see e.g. Stenflo 1994; Bommier 1997). Note however that the non-magnetic redistribution matrix of Eq. (9) becomes more complicated in the context of approximation level III of Bommier (1997) in the presence of magnetic fields, because a structuring with different domains need to be introduced in the (x, x') frequency space. Still, apart from second order effects, it is sufficient to account for a weak turbulent magnetic field simply by reducing the value of W_2 according to Eq. (16) without having to deal with the structuring in (x, x') space.

To explore the coupling between line and continuum we introduce the difference

$$\Delta p(W_2) = \frac{1}{W_2}\left(p_{W_2} - p_{W_2=0}\right). \qquad (17)$$

The variable p_{W_2} represents the total degree of polarization Q/I in a line with intrinsic polarizability W_2. The emergent polarization for exactly the same line but with $W_2 = 0$ is denoted $p_{W_2=0}$. Dividing the difference by W_2 allows us to explore how the emergent polarization scales over a large range of W_2 values. From Fig. 6 we see that Δp represents the intrinsic line polarization that is linearly added on top of the purely depolarizing line with $W_2 = 0$.

The degree of coupling between line and continuum can be judged by comparing with a special case. If we would neglect the continuum polarization, all the emergent polarization would be exclusively due to the intrinsic line polarizability, and $p_{W_2=0}$ would be identically zero. We get this case by first increasing $\kappa_{\rm c}$ by $(\kappa_{\rm c} + \sigma_{\rm c})/\kappa_{\rm c}$ and subsequently setting $\sigma_{\rm c} = 0$. Then we have removed scattering from the continuum while maintaining the same total opacity.

Figure 7 gives Δp (polarization in percent) for $W_2 = 0.01$ (solid), $W_2 = 0.50$ (dotted), and $W_2 = 1.00$ (dashed), while accounting for the polarization of the continuum. Each line is overplotted with the results for a second case marked by the filled circles. It is the special case that is obtained by neglecting the continuum polarization. The perfect fit between the curves and the filled circles proves that the intrinsic line polarization can be dealt with independently from the continuum polarization. Depolarization needs to be represented correctly by the $W_2 = 0.00$ curve, but any intrinsic line polarization is just a linear superposition on top of this curve. The coupling between intrinsic line polarization and the continuum opacity may thus be neglected.

In Fig. 7 we notice that the scaling of the line polarization with W_2 is not perfectly linear. To explore this scaling property we compare the line center ($x = 0$) values of $\Delta p(W_2)$ in Fig. 7 for different W_2. Let us introduce the quantity

$$\delta = \frac{\Delta p(W_2)}{\lim_{W_2 \to 0} \Delta p(W_2)}, \qquad (18)$$

where $\Delta p(W_2)$, defined by Eq. (17), is evaluated at $x = 0$. The denominator of Eq. (18) can be approximated by the line center value of the solid curve in Fig. 7, while the numerator corresponds to $\Delta p(W_2)$ (again at line center) for any W_2. A value $\delta = 1$ for all W_2 would represent a linear scaling of the line polarization with W_2.

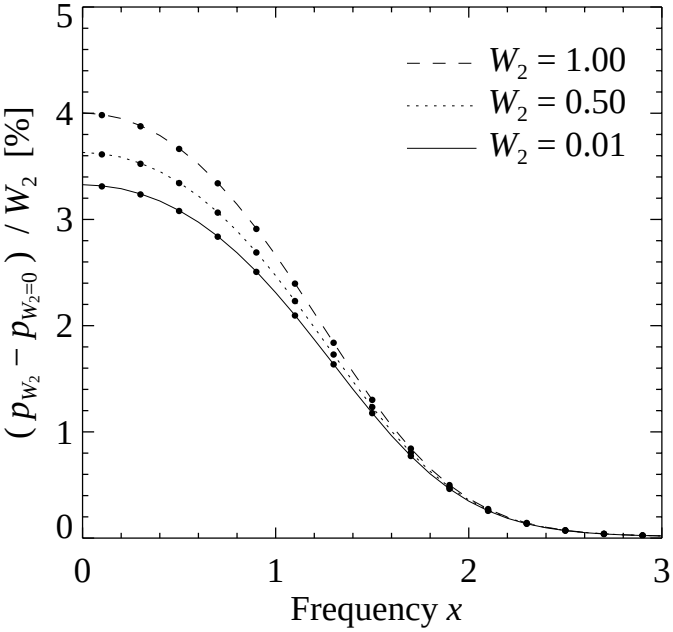

Fig. 7. The polarization of the Fe I line with a polarized continuum when W_2 is 0.01 (solid), 0.50 (dotted), and 1.00 (dashed) relative to its value when $W_2 = 0.0$. These curves coincide with the degree of line polarization that are obtained when the continuum polarization is neglected (filled circles). This demonstrates that the continuum polarization does not couple to the intrinsic line polarization.

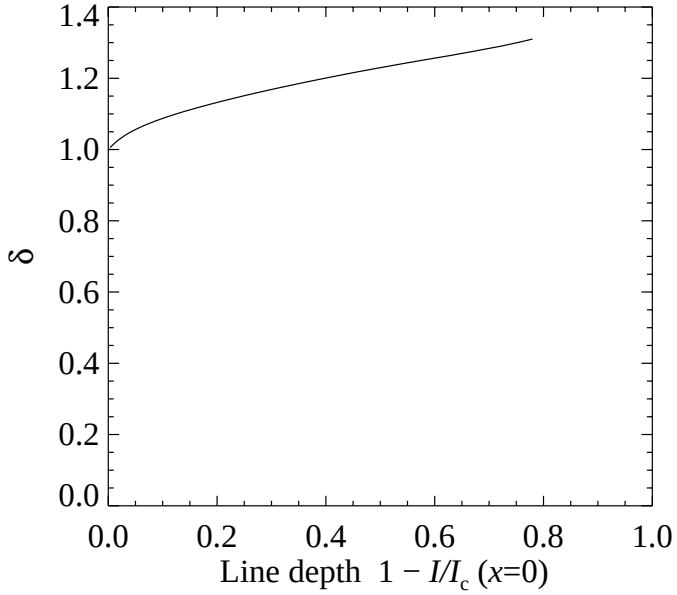

Fig. 8. Influence of W_2 and optical thickness of the line on the scattering polarization. δ, defined by Eq. (18), has been calculated for a set of lines of the Fe I type. The different lines are obtained by scaling the line opacity with a depth independent factor, which results in different intensity line depths. A value $\delta = 1$ represents the case that the emergent line polarization increases linearly with W_2. This value is only approached for very thin lines. The stronger the line, the faster the polarization increases with increasing W_2.

In the following we compute the quantity δ for a whole set of "Fe I" lines, all for an intrinsic line polarizability $W_2 = 1$ (in the numerator of Eq. (18)). These "Fe I" lines differ only in the line opacity κ_ℓ, which is scaled with a depth independent factor. This allows us to compute different lines with comparable parameters that vary only in the optical thickness. The larger the line opacity the larger is the resulting line depth in intensity.

Figure 8 shows δ as a function of line depth for this set of "Fe I" lines. When the line depth decreases, δ approaches 1, which means that the line polarization for optically very thin lines scales linearly with W_2. The nonlinearity with W_2 appears only for stronger lines, increases with line depth, and is therefore due to optical thickness effects.

Our calculations and Fig. 8 thus indicate that the nonlinear scaling with W_2 can be understood in terms of multiple scattering. Obviously the last scattering process is the most relevant for the emergent polarization. However, the larger the line opacity due to scattering, the more scattering events occur. Therefore the incident radiation field at the last scattering process is already partialy polarized, which leads to an additional increase of the emergent polarization. As the influence of multiple scattering is more pronounced for stronger lines, we obtain the monotonic growth of δ in Fig. 8.

The observed W_2 scaling properties depend on the details of line formation. While the "Fe I" lines should be representative for most real solar lines, it is possible to construct cases with a different behavior. If we do the analysis of Figs. 7 and 8 not for the Fe I line but for the "0 km" scattering line of Fig. 2 (this time with $W_2 \geq 0$), we find that the intrinsic line polarization scales exactly linearly with W_2 and that only the last scattering process contributes to the observed polarization. That line is formed very deep in the atmosphere where the continuum absorption is still relevant. Therefore, all the line polarization formed before the last scattering process is destroyed again, in contrast to the Fe I line.

5. Conclusions

Our analysis of depolarizing lines in the solar spectrum has allowed us to make a parameter survey of their behavior. We find that the amount of depolarization is not well correlated with the line depth in the intensity spectrum. Different lines with the same depth in Stokes I can both cause complete and barely visible depolarization, depending on the details of line formation. In particular we have shown that for absorption lines the depolarization decreases rapidly with height of formation, if the intensity line depth is kept fixed. The opposite behavior is found for pure scattering lines, which depolarize very strongly if they are formed high in the atmosphere.

We have identified the relevant physical processes causing depolarization. First we have studied lines with no intrinsic polarization. As is well known, the presence of an anisotropic radiation field is necessary to obtain scattering polarization. The line opacity influences and in general reduces the anisotropy of the radiation field in the line core, which results in smaller core polarization than in the continuum. This can however only partially explain the amount of depolarization in different lines. In the case of lines for which the atmosphere is optically thick below their height of formation, another relevant parameter is the probability that a photon is scattered above the height where

the atmosphere becomes optically thin. This probability scales with the path length inside the optically thin slab in the direction of the line-of-sight. It is smaller in the line core than in the continuum, which naturally leads to a smaller degree of polarization in the line. For optically thin lines formed high in the atmosphere the depolarizing behavior is different for absorption and scattering lines. An absorption line filters out Stokes I and Q by the same fraction, leaving the degree of polarization unchanged. A scattering line (with $W_2 = 0$) reduces primarily Stokes Q and causes strong depolarization.

In a second part we have examined lines with intrinsic polarization. The total polarization is due to the combined effect of continuum polarization, depolarization, intrinsic line polarization, and possibly further depolarization due to the Hanle effect. A turbulent magnetic field would have the same effect as reducing the value of W_2, a case that is covered by our analysis. We show that the coupling between continuum and intrinsic line polarization is very weak and can safely be neglected. If the polarization profile shape of a line with $W_2 = 0$ that depolarizes the continuum polarization is known, the intrinsic line polarization of the same line (but with a non-zero W_2) can just be linearly added.

We have found that the intrinsic line polarization does not scale entirely linearly with W_2. The (fairly small) deviation from linearity can be understood in terms of multiple scattering. The polarization increases with W_2 faster than linearly if more than the last scattering process contributes to the formation of the emergent polarization.

The new insight that we have gained through the present work represents a necessary step in understanding and making diagnostic use of the richly structured "second solar spectrum". For magnetic-field diagnostics with the Hanle effect we need to extract the intrinsic line polarization from the observed mixture of line and continuum. The various contributions from continuum polarization, intrinsic line polarization, magnetic-field effects, and non-magnetic depolarization are generally of the same order of magnitude and exhibit spatial and temporal variations. While this combination of effects greatly complicates the interpretation, it provides us with potentially rich diagnostic opportunities that have yet to be exploited.

Acknowledgements. We thank M. Faurobert for comments that helped to improve the manuscript. Support for the work of D. M. Fluri has been obtained through grant No. 20-64945.01 from the Swiss National Science Foundation, which is gratefully acknowledged.

References

Bommier, V. 1997, A&A, 328, 726
Carlsson, M. 1986, Upps. Astron. Obs. Rep., 33
Faurobert-Scholl, M., Frisch, H., & Nagendra, K. N. 1997, A&A, 322, 896
Fluri, D. M., & Nagendra, K. N. 2003, A&A, in press
Fluri, D. M., & Stenflo, J. O. 1999a, A&A, 341, 902
Fluri, D. M., & Stenflo, J. O. 1999b, in Solar polarization, Proc. 2nd SPW, ed. K. N. Nagendra, & J. O. Stenflo (Kluwer, Dordrecht), ASSL, 243, 171
Fluri, D. M., & Stenflo, J. O. 2001, in ed. M. Sigwarth, Advanced Solar Polarimetry – Theory, Observations, and Instrumentation, ASP Conf. Ser., 236, 205
Fontenla, J. M., Avrett, E. H., & Loeser, R. 1993, ApJ, 406, 319
Gandorfer, A. M. 2000, The Second Solar Spectrum, vol. I: 4625 Å to 6995 Å, ISBN No. 3 7281 2781 7, VdF, Zurich
Gustafsson, B. 1973, Upps. Astron. Obs. Ann., 5(6)
Hummer, D. G. 1962, MNRAS, 125, 21
Ivanov, V. V. 1991, in ed. L. Crivellari, I. Hubeny, & D. G. Hummer, Stellar Atmospheres: Beyond Classical Models, Proc. NATO (Kluwer, Dordrecht), 81
Landi Degl'Innocenti, E. 1984, Sol. Phys., 91, 1
Mihalas, D. 1978, Stellar Atmospheres, Freeman and Company, San Francisco, 2nd edition
Nagendra, K. N., Frisch, H., & Faurobert-Scholl, M. 1998, A&A, 332, 610
Nagendra, K. N., Frisch, H., Faurobert-Scholl, M., & Paletou, F. 2000, J. Astrophys. Astr., 21, 255
Nagendra, K. N., Paletou, F., Frisch, H., & Faurobert-Scholl, M. 1999, in ed. K. N. Nagendra, & J. O. Stenflo, Solar polarization, proc. 2nd SPW (Kluwer, Dordrecht), ASSL, 243, 127
Nagendra, K. N., & Stenflo, J. O. 1999, Solar polarization, proc. 2nd SPW (Dordrecht, Kluwer), ASSL, 243
Olson, G. L., Auer, L. H., & Buchler, J. R. 1986, J. Quant. Spectrosc. Radiat. Transfer, 35, 431
Paletou, F., & Faurobert-Scholl, M. 1997, A&A, 328, 343
Stenflo, J. O. 1982, Sol. Phys., 80, 209
Stenflo, J. O. 1994, Solar Magnetic Fields (Kluwer, Dordrecht)
Stenflo, J. O., & Keller, C. U. 1996, Nature, 382, 588
Stenflo, J. O., & Keller, C. U. 1997, A&A, 321, 927
Stenflo, J. O., Keller, C. U., & Gandorfer, A. 1998, A&A, 329, 319
Stenflo, J. O., & Nagendra, K. N. 1996, Solar polarization, proc. 1st SPW (Dordrecht, Kluwer), Sol. Phys., 164
Stenflo, J. O., Twerenbold, D., & Harvey, J. W. 1983a, A&AS, 52, 161
Stenflo, J. O., Twerenbold, D., Harvey, J. W., & Brault, J. W. 1983b, A&AS, 54, 505